Slab Models for Classical Diffusion in the Belt Pinch

Glenn Bateman

IPP 1/131 March 1973

MAX-PLANCK-INSTITUT FÜR PLASMAPHYSIK

GARCHING BEI MÜNCHEN

MAX-PLANCK-INSTITUT FÜR PLASMAPHYSIK

GARCHING BEI MÜNCHEN

Slab Models for Classical Diffusion in the Belt Pinch

Glenn Bateman

IPP 1/131 March 1973

Die nachstehende Arbeit wurde im Rahmen des Vertrages zwischen dem Max-Planck-Institut für Plasmaphysik und der Europäischen Atomgemeinschaft über die Zusammenarbeit auf dem Gebiete der Plasmaphysik durchgeführt.

IPP 1/131 Glenn Bateman

Slab Models for Classical Diffusion in the Belt Pinch.

(in English)

March 1973

Abstract

Classical diffusion is considered as a time dependent and self consistent problem for a free-boundary plasma in the plane slab and cylindrical slab geometries. These conditions approximate the Belt Pinch experiment. It is found that the instantaneous diffusion rate changes rapidly as the plasma spreads and the fields decay. There is a succession of at least four physical phenomena which can dominate under different conditions: The poloidal electric field decays rapidly during an initial, finite-β, transient stage. The pinch effect induced by the toroidal electric field may impede diffusion for an intermediate time span. After the pinch effects become negligible, Spitzer diffusion induces a pressure decay which is algebraic with time and a poloidal B-field decay which is exponential with time. Although the pressure decay is initially faster, the rates soon become comparable. The Pfirsch-Schlüter effect enhances this diffusion only late in the discharge after the plasma has spread out and the rotational transform has decayed.

A formula is also found for the radial position of the cylindrical slab as the fields decay. For passive field programming, there is a fixed but unstable position.

I. Introduction

Classical plasma diffusion / see for example 1 - 17 / embodies a variety of physical processes. Here we shall consider the combination of "Spitzer" diffusion, the pinch effect, flow fields resulting in the Pfirsch-Schlüter effect, and the resistive decay of the fields. Our physical understanding of these effects can be developed by considering them one at a time before combining them in a self-consistent theory. More effects come from the evolution of the plasma shape and the evolution of the fields driven by the external circuitry. For the present work, these effects will be reduced to their simplest form by considering only one dimensional models (plane and cylindrical slab), free plasma boundary (with no plasma loss from the system), and perfectly conducting outer walls.

The goal of this work is to understand the slowest stages of diffusion in the Belt Pinch /18/. To this end, our assumptions will be tailored to the following observations of the Belt Pinch plasma.

After the initial shock heating and a transient axial contraction phase, the Belt Pinch operates like a Tokamak since it is an axisymmetric toroidal plasma in which the magnetic fields necessary for equilibrium are maintained by plasma currents. However, the Belt Pinch differs from most Tokamaks in the following ways:

1) The plasma cross section is highly elongated (presently about 40 cm high, several cm thick, and 22 cm major radius). For a given rotational transform $\iota/2$/(kept below the Kruskal-Shafranov limit $\iota < 1$ in experiments) the elongated plasma has larger poloidal B-field (short way around) and larger toroidal current density (long way around) than a circular plasma with the same thickness and applied toroidal B-field. This results in higher β and a faster Ohmic heating rate. For reasons associated with the shock heating, the initial β and density ($n_e \sim 10^{16}$) are high compared to circular Tokamaks. Hence a fully applicable theory should be self-consistent at finite β. In this work, finite β effects are estimated; but the analysis used to reduce the partial differential equations to ordinary differential equations is generally valid for $\beta \sim O(.1)$.

   Hence we confine most of our attention to the later stages of the Belt Pinch discharge.

2) There is no tangible limiter to define the edge of the Belt Pinch plasma; the visible plasma is well separated from the glass discharge tube and appears to change shape and spread over time. There might be a distinct vacuum region sharply distinguished from the plasma region by a separatrix. As yet, there is no satisfactory equilibrium theory to describe the evolution of such an elongated plasma shape as the plasma currents and coil currents change. Recent computer calculations by Lackner, v.Hagenow and Ochem have just begun to simulate the Belt Pinch equilibrium /19,20/.

However, it is necessary to have this global information for a self consistent diffusion theory. For the present work we shall use the simplest model of an infinite slab with free boundary surrounded by vacuum magnetic fields. It will be assumed that no plasma is lost to the system so that the amount of plasma per unit length is fixed as the slab spreads in thickness. The alternative possible assumption of a fixed plasma boundary across which plasma is lost leads to a steepening of the pressure profile near the edge; then the use of series expansions around the plasma center is no longer feasible.

3) The toroidal current decays during the observed plasma life time because there is no iron core transformer (present in most Tokamaks). Hence the theory must be time-dependent.

4) The present Belt Pinch operates at low temperatures (typically 10 eV). We believe that this temperature is determined by the balance between Ohmic heating and radiation from impurity spectral lines /21,22/ and that this balance is achieved on a time scale of less than 10 μsec (compared with the observed plasma life time of 50 - 100 μsec). This "radiation barrier" is a steep function of temperature. Hence, the local plasma temperature should be even more uniform than would be expected from the effect of heat conduction alone /4/ and it should be nearly constant in time as other parameters vary over some range. It does not seem worth while to make more detailed calculations of temperature profiles and their effects because the impurity level is not accurately known and the nature of impurity radiation cooling is not precisely known.

For the purpose of estimation, an example of the radiation barrier due to the presence of Oxygen impurity under Belt Pinch conditions has been prepared by W. Engelhardt /22/

and is shown in Fig.1. We believe that it is misleading to use the equilibrium values of the ionization stages for a calculation of the radiation barrier. Rather, one should use the degree of ionization appropriate to the time scale over which a given temperature and density range has been held. Using the calculation by W. Lotz /23/ for T_e = 10 eV and $n_e = 10^{16}$ the ionization time scales are: O_I, .01 µsec; O_{II}, .33 µsec; O_{III}, 5 µsec; O_{IV}, 100 µsec; etc. These figures are very sensitive to the temperature. An experimental observation /24/ at 10 µsec for a Belt Pinch discharge where T_e was below 10 eV indicated that the Oxygen impurity was almost completely in the O_{II} stage. However, the cooling rates for the ionization stages O_{II} through O_{VI} are very similar. For comparison, the Ohmic heating rate in the center of the plasma is shown (straight lines in Fig.1) based on the formula

$$\frac{1}{T_e} \quad \frac{dT_e}{dt} \; [\mu sec]^{-1} = 3.43/T_e^{3/2} \; [ev] \; \Delta^2 \; [cm]$$

where Δ is the slab thickness. This formula assumes a parabolic pressure profile (see Section III) to determine the current density as a function of the external poloidal field and assumes that the central plasma pressure is balanced by the external poloidal field. Where the Ohmic heating curve is below the radiation cooling curve the plasma cools at a rate determined by the difference between the curves. Intersections on the left side of the radiation curve determine stable temperatures while intersections on the right side (not possible with this particular curve) are unstable to temperature changes. For stable temperature points, the temperature changes little with moderate changes of Δ and n_e - especially of the density decreases as the plasma spreads (the radiation rate for a given ion is proportional to the impurity ion density).

5) Neoclassical effects are expected to set in at electron temperatures of about 400 ev for the Belt Pinch geometry and density /25/. Hence classical diffusion should apply to this and the next generation of Belt Pinches.

These are the relevant features of the Belt Pinch. Motivated by these observations we construct the following model suitable for analysis: We consider a slab-like plasma with uniform and constant temperature, free boundary, and naturally decaying fields. The mathematical model consists of the moment equations /26/ and pre -Maxwell equations (without displacement current) /27/.neglecting inertial terms, viscosity, and charge separation. These and the other assumptions involved in the reduction of the moment equations (mass and momentum) are discussed in Appendix A. This results in the standard equations

$$\nabla \cdot B = o \tag{1}$$

$$J = \nabla \times B \tag{2}$$

$$\nabla p = J \times B \tag{3}$$

$$\frac{1}{S}\left[J - (1 - C)\,\frac{J \cdot B}{B^2} B\right] = cE + v \times B \tag{4}$$

$$\frac{\partial B}{\partial t} = - \nabla \times cE \tag{5}$$

$$\frac{\partial p}{\partial t} = - \nabla \cdot (pv) \tag{6}$$

$$C \equiv \eta_{\|}/\eta_{\perp} = 0.51 \text{ for } Z = 1$$

$$S \equiv \omega_{pe}^2\, \tau_e/c^2 = 0.124\, (T_e[\text{ev}])^{3/2}\ \mu\text{sec/cm}^2.$$

Here $S = 1/c\eta_{\perp}$ provides the basic time /(length)^2 scale for diffusion. The current and pressure have been rescaled $j[\text{esu}] \to J\, c/4\pi$, $p \to p/4\pi$.

The pressure balance equation (3) and Ohm's Law Eq.(4) are derived from the equations of motion for electrons and singly charged ions.

To derive Eq.(3) we neglected the inertial term, which scales like the ion transit time divided by the diffusion time over a corresponding distance, and a charge separation term, which scales like the Debye length divided by plasma thickness. To derive Eq. (4), the Hall current was expressed as a gradient (using Eq.(3) and uniform temperature) and absorbed into the electric field - the new electric field has no component normal to the flux surfaces.

In section II, the plane slab diffusion is considered in a number of limiting cases and a set of ordinary differential equations is derived for the evolution of the pressure and the B-fields. In section III, the corresponding equations are derived for the infinite cylindrical slab and the models are compared using a representative set of computer solutions.

The plane slab is treated most extensively because its analysis is the cleanest and the limits of applicability can be most clearly defined. The infinite cylindrical slab exhibits the Pfirsch-Schlüter effect and also the radial drift of the plasma, as flux diffuses through it, without the complications of a separatrix and special coils that surround the finite length equilibrium.

However, both slab models are mathematically singular approximations to finite plasmas geometries. Some of the fundamental mathematical problems are discussed in Appendix B.

II. Plane Slab

There is a surprising variety of physical phenomena to be found in even this simplest one dimensional diffusion model. Furthermore, we shall see that the plane slab results provide a good approximation to the cylindrical slab diffusion under those conditions where the Pfirsch-Schlüter effect can be neglected.

The conventions and notation are illustrated in Fig.2. The system is symmetric across $x = 0$. There is a vacuum between the edge of the plasma $x_e(t)$ and a perfectly conducting (flux preserving) wall at fixed position x_w ($E(x_w) = 0$). In the vacuum there is an externally imposed fixed B_{ye} field. For ease of comparison with later models, this will be called the "toroidal field". The other field component, "poloidal field" $B_{ze}(t)$ in the vacuum is entirely due to plasma currents. Inside the plasma, both field components $By(x,t)$ and $B_z(x,t)$ are altered by plasma currents. At $x = 0$, the boundary conditions for the B-field, current, E-field, diffusion velocity (x-component) v and pressure are

$$B_z = J_z = E_z = v = 0$$

$$\partial B_y/\partial x = \partial J_y/\partial x = \partial E_y/\partial x = \partial p/\partial x = 0.$$

Since all B-field lines are straight in the plane slab model, the pressure balance equation is an exact differential

$$d\,(2p + B_y^2 + B_z^2) \,/\, dx = 0. \qquad (7)$$

There is a discontinuity in the conductivity, and hence also in the current, at the edge of the plasma. For this reason, it is convenient to use the integral form of Faraday's law, Eq.(5), using fluxes defined by

$$B_z \equiv -\partial\Psi_z/\partial x \;;\quad \Psi_z(x_w) = 0$$
$$B_y \equiv \partial\Psi_y/\partial x \;;\quad \Psi_y(o) = 0 \qquad (8)$$

when Ψ_z is the poloidal flux between the outer wall and any plane x, and Ψ_y is the toroidal flux between the center of the plasma and any plane x.

Using the assumption that the wall is a perfect conductor and again assuming symmetry,

$$E_y(x_w) = 0 \;;\quad E_z(o) = 0,$$

we have the integral form of Faraday's law

$$\partial\Psi_z/\partial t = c\,E_y \;;\quad \partial\Psi_y/\partial t = c\,E_z. \qquad (9)$$

Before proceeding by formal expansion to a full solution of Eqs. (1), (2), (4), (6), (7) and (9), let us consider several extreme cases by making special selections for the dominant terms.

Consider the field decay within an isotropic rigid plasma ($C = 1$, $v = 0$). The toroidal B_y field may be decomposed into a uniform part plus a set of simple harmonics $\cos((2n+1)\pi x/2x_e)$ representing the dip of the toroidal field within the plasma. Then each harmonic decays exponentially with e-folding time

$$\tau_n = x_e^2\, S\, (2/(2n+1)\pi)^2. \qquad (10)$$

These time scales for the decay of the poloidal current are the fastest diffusion time scales - they will be considered transients here. The decay of the poloidal B_z field is not so simple. However, if the plasma is thin by comparison to the wall distance

$$\alpha \equiv x_e/x_w \ll 1, \qquad (11)$$

there is a large reservoir of poloidal field energy by comparison to plasma energy. Then the time scale for the decay of the poloidal B_z-field, as well as the toroidal current and electric field, is

$$\tau_{pol\ B} \sim x_w\, x_e\, S. \tag{12}$$

More detailed studies of such decay times (for circular cross sections) have been made by Hobbs /28/.

The above applies to a rigid plasma; now consider an expanding plasma and neglect the electric fields.

For this extreme case we suppose that the plasma is contained by the dip in the toroidal field which, in turn, is produced by a poloidal current driven by the diffusion velocity crossed with the toroidal B-field.

Pressure balance and Ohm's law become

$$2p \simeq B_{ye}^2 - B_y^2 \tag{13}$$

$$J_z \simeq S\, v\, B_y. \tag{14}$$

These approximations (using $\eta_{\parallel}/\eta_{\perp} = 1$ here) can be shown, <u>a posteriori</u>, to be equivalent to the assumptions

$$\gamma \ll \beta_y \ll 1 \tag{15}$$

where

$$\beta_y(x,t) \equiv 2p(x,t)\, B_{ye}^2 \tag{16}$$

$$\gamma(x,t) \equiv B_z^2(x,t) \,/\, B_{ye}^2. \tag{17}$$

v is the diffusion velocity. Using Eq.(14), v can be eliminated from the equation of continuity to yield

$$\frac{\partial \beta_y}{\partial t} = \frac{1}{2S} \frac{\partial}{\partial x} \left(\beta_y \frac{\partial \beta_y}{\partial x}\right). \tag{18}$$

In the low-β limit, $v B_z$ has little effect on the toroidal current J_y [from Eq.(4)]. Hence the decay of the poloidal B-field proceeds as described in the last paragraph

$$\frac{1}{B_{ze}} \frac{\partial B_{ze}}{\partial t} = - \frac{1}{2 x_e x_w S} \tag{19}$$

The time scale for the decay of β_y as given by Eq.(18) is

$$\tau_\beta \sim x_e^2 \, S / \beta_y . \tag{20}$$

Hence β_y may initially decay faster than B_z; but as β_y decreases and x_e increases, β_y ultimately decays slower than B_z. A nonlinear diffusion equation such as Eq.(18) typically leads to <u>algebraic</u> decay in time for β_y while a linear equation such as Eq.(19) typically leads to exponential decay in time for B_{ze}.

One way to study diffusion equations like Eq.(18) is to look for "similarity solutions" - special solutions composed of combinations of functions of one variable with the appropriate arguments. These functions then satisfy ordinary differential equations. Classes of similarity solutions for a number of equations like Eq.(18) were exhaustively studied by Holladay /29/. In particular, he classified the solutions according to the boundary conditions to which they were appropriate. Rosenbluth and Kaufman /3/ applied the similarity solution technique to a larger system of diffusion equations, which contained Eq. (18), to describe the spreading of a semi infinite plasma. They found the $t^{-1/3}$ decay behaviour which we shall soon discuss. Grad /12 (section VI)/ pointed out that if a similarity solution for Eq. (18) is perturbed the eigenfunctions all decay algebraically. Also, if β_y is held to zero at a <u>fixed</u> boundary it must have an infinite slope there ($\beta_y \sim (1-x/x_e)^{1/2}$) representing a flow of plasma across the boundary. The free-boundary solution, with finite slope at the edge and no plasma loss, is fundamentally different from the fixed boundary solution.

For the free boundary problem where the total amount of plasma is conserved ($x_e(t)\ \beta_y(o,t) = \text{const.}$), the simplest similarity solution to Eqs. (18) and (19) is

$$\beta_y = \beta_{yo}\ \tau^{-1/3}\left[1 - x^2/a^2(t)\right] \tag{21}$$

$$x_e(t) = a(t) = a_o \tau^{1/3} \tag{22}$$

$$B_z(x,t) = \frac{x}{a} B_{ze}(t=o)\ \exp\left[-\frac{1}{2\beta_{yo}} \frac{a_o}{x_w} (\tau^{2/3} - 1)\right] \tag{23}$$

where τ is a linear function of time

$$\tau \equiv 1 + \frac{3\ \beta_{yo}\ t}{a_o^2\ s} \quad . \tag{24}$$

Note that B_z does not have a simple exponential decay, but rather $\exp\ (-\ (t/t_o)^{2/3}\ )$. Still the B_z field ultimately decays faster than the plasma pressure; the initial ordering $\gamma \ll \beta_y \ll 1$ may be violated for an intermediate time interval (limiting profile) but it is ultimately recovered again. This pattern is illustrated in Fig.(3) where the normalized solutions [Eqs. (21) and (23)] are plotted for the particular choice of damping decrement $a_o/2\ \beta_{yo}\ x_w = .05$ and for the time scale $t/\ 4\ x_w^2 s$. This corresponds to the same conditions as in Fig.(8a) (dashed curve). The poloidal field decays a little more slowly in Fig.(8a) because of another effect which is discussed at the end of this section.

For this particular choice of similarity solution, Eqs. (21) to (24), β_y has a parabolic profile in x. Consider now a perturbation from this solution and the corresponding linearization of Eq.(18). Like β_y, the perturbation must be even in x and so may be expressed as the sum over even powers of x. Using $a(\tau)$ given by Eq.(22), since the perturbation should not greatly affect the plasma spreading, the perturbation is found to have the form

$$\sum_p \beta_{2p}\ \tau^{-(2p^2\ -\ p+1)/6}\ \ (x/a(\tau))^{2p}$$

Since these terms decay much more rapidly than the parabolic form Eq.(21), for $o < x < a(\tau)$, we conclude that the parabolic form becomes the most likely diffusion profile after a few multiples of the initially fast diffusion time scale, Eq.(20). This is an important observation because most of the rest of our analysis relies on the first few terms of a power series in x. In general, estimates like this may help support the often used assumption in equilibrium calculations that p is a linear function of Ψ.

We have seen that there is an initial transient stage characterized by a strong poloidal electric field followed by a stage in which poloidal currents are maintained by a v x B driving term thus forcing β_y to decay algebraically. These stages are characterized by $\beta_y \sim O(1)$ and $\gamma \ll \beta_y \ll 1$ respectively. But since β_y initially decays faster than γ there are initial conditions after which β_y becomes comparable to or less than γ for some finite time domain. Under these conditions the system approaches a third extreme case called the "limiting profile" /8, 11, 12/. The profiles for this extreme case are calculated by letting $x_w \to \infty$ so that the poloidal field B_{ze} is constant in time. This is equivalent to having an infinite reservoir of poloidal flux.

In this case there exists a steady state, static solution to Eqs. (1), (2), (4), (6), (7) and (9) with <u>no</u> sources or sinks of plasma. Physically, the E x B drift inward (pinch effect) just balances the diffusion outward. Here the poloidal E_z-field has decayed away leaving only a uniform toroidal E_{yo}-field. The equations for the resulting B-fields, valid for arbitrary β and E_{yo}-field, are

$$\left.\begin{aligned} \frac{d B_z}{dx} &= - \frac{Sc\, E_{yo}}{C} \frac{1 + C B_z^2/B_y^2}{1 + B_z^2/B_y^2} \\ \frac{d B_y^2}{dx} &= + 2 B_z \frac{Sc\, E_{yo}}{C} \frac{1 - C}{1+B_z^2/B_y^2} \end{aligned}\right\} \qquad (25)$$

In the low β limit, $B_z^2 \ll B_y^2$, the solution is

$$B_z = B_{ze}\, x/x_e \quad ; \quad B_{ze} = -\frac{S\, c\, E_{yo}}{C}\, x_e$$

$$B_y^2 = B_{ye}^2 + B_{ze}^2 (1 - C)\,(1 - x^2/x_e^2) \qquad (26)$$

$$p = \frac{B_{ze}^2}{2}\, C\,(1 - x^2/x_e^2).$$

In the $\beta = 1$ limit, the analytic solution (which corresponds to the z-pinch)

$$B_z = -\frac{Sc\, E_{yo}}{C}\, x \quad ; \quad B_y = 0 \qquad (27)$$

also has a parabolic profile for $p(x)$.

Surprisingly, computer solutions of Eq. (25) for arbitrary β all have nearly parabolic profiles for $p(x)$. A representative example is shown in Fig.(4).

A property common to all of the limiting profiles is that the plasma is diamagnetic with respect to the poloidal B_z-field and paramagnetic with respect to the toroidal B_y-field. The toroidal B-field, which is necessary for MHD stability, effectively excludes part (half) of the plasma. This peculiar effect is due to the difference between parallel and perpendicular resistivity - the fact that both components of the current are driven by one component of the E-field. This effect was predicted and experimentally observed by Bezbachenko /30/ and by Bickerton /31/. More recently it was observed in the TESI experiment at Jülich /32,33/. The effect is enhanced by high-Z impurities; $C \to 0.29$ as $Z \to \infty$ so that more than two thirds of the plasma is excluded relative to purely poloidal field confinement. We shall see later that the paramagnetic effect ($\beta_y < \gamma$) may be greatly enhanced by Pfirsch-Schlüter diffusion.

The solutions that have been considered so far in various limits

are all essentially parabolic in x for β_y and linear in x for B_z. We shall now use this approximation to reduce the full set of partial differential equations [(1) - (6)] to ordinary differential equations. The instantaneous decay rates and full evolution of p(o,t) and $B_{ze}(t)$ are then determined from these equations by numerical computation. The alternative procedure of finding a variational minimum principle for the original partial differential equations and then deriving ordinary differential equations for the evolution of parameters in test functions /34/ would be preferable; but this procedure has not been sufficiently developed yet. A computer solution of the original partial differential equations is beyond the scope of this work and is a technique that cannot be readily applied to more complicated geometries.

The spatial derivatives in the diffusion equations bring down higher order terms in the expansion. The lowest order equations then give relations among the lowest two orders of the unknowns. At any level of truncation, there are more unknowns than equations. We shall complete the system by using the following global constraints:

At the plasma surface the fluxes and B-fields are matched to their vacuum values. In particular the poloidal flux in the vacuum is

$$\Psi_{ze}(t) = B_{ze}(t)\ (x_w - x_e(t)). \tag{28}$$

and the B_y-field is fixed in the vacuum.

After eliminating unknowns, the four matching conditions (flux and poloidal B-field at the two edges of the plasma) yield two new equations. Next, the pressure is assumed to be parabolic out to the edge of the plasma and to be zero there

$$p\ (x,t) = p_o(t)\ (1 - x^2/x^2_e\ (t)). \tag{29}$$

Finally, it is assumed that the total amount of plasma per unit area of slab is fixed

$$p_o(t)\ x_e(t) = \text{const.} \tag{30}$$

The resulting ordinary differential equations are

$$\frac{1}{B_{ze}}\ \frac{d\,B_{ze}}{d\tau} = W_{bz} = W_{\psi z} - \frac{a}{1-a}\ W_p \tag{31}$$

$$\frac{1}{p_o}\ \frac{d\,p_o}{d\tau} = W_p \equiv W_{sp} + W_{ey} + W_{ez}. \tag{32}$$

Using dimensionless forms for time and the plasma half-thickness

$$\tau \equiv t/4x_w^2 S \qquad\qquad a \equiv x_e(t)/2x_w \tag{33}$$

we find the decay rate for the external poloidal flux

$$W_{\psi z} = -\ ^{2\,C}/_{a(1\,-\,a)} \tag{34}$$

which is used in Eq.(31) for the decay rate of the B_{ze}- field.

The decay rate for the central plasma pressure is the sum of Spitzer diffusion

$$W_{sp} = -\ 2\ p_o/B_{yo}^2\ a^2 \tag{35}$$

the E_y x B_z pinch effect

$$W_{ey} = C\ B_{ze}^2/\ B_{yo}^2\ a^2 \tag{36}$$

and the E_z x B_y pinch effect

$$W_{ez} = \left[B_{ze}^2\ W_{\psi z} - \left(p_o + \frac{a}{1-a}\ B_{ze}^2\right)\ (W_{sp}+W_{ey})\right] \Big/ \left[B_{yo}^2 + p_o + \frac{a}{1-a}\ B_{ze}^2\right] \tag{37}$$

For a given toroidal field in the vacuum, B_{ye}, the toroidal field in the center of the plasma, B_{yo}, is determined from the pressure balance equation

$$B_{yo}^2 = B_{ye}^2 + B_{ze}^2 - 2\ p_o. \tag{38}$$

The solution $B_{ze}(t)$ and $p_o(t)$ of Eqs. (31-32) are represented by the dashed curves in Figs. (6a-8a), and the corresponding decay decrements [Eqs. (35-37)] are plotted in Figs. (6c-8c). In all these graphs we set $B_{ye} = 1$, $a(t=0) = .02$ and $p_o(t = o) = .2$

while different initial values of B_{ze} are used. Note that the vertical scale is logarithmic and the time scale $t/4x_w^2 S$ is used on the horizontal axis. In all of the cases studied so far, the $E_z \times B_y$ pinch effect yields a negligible decay decrement by comparison to the others - rough estimates indicate that it is a finite β effect. Note that the final value of $p_o(t)$ is nearly the same in all three graphs as would be suggested by the analytic solution Eq.(2) provided the pinch effects are only transient. However, the poloidal field $B_{ze}(t)$ decays less rapidly than the analytic solution [Eq.(23)] because of the second term in Eq. (31). This term came about because the flux in the vacuum region changes not only because the B-field changes but also because the dimensions of the vacuum region change. In this case, the time rate of change of the inductance effectively reduces the plasma resistance.

At the end of section III, these results are compared with the cylindrical slab results.

III. Cylindrical Slab

Two new effects appear when the plane slab is bent into an infinite cylindrical slab - a Belt Pinch without end effects. Plasma spreading is enhanced by the Pfirsch-Schlüter effect /5, 6, 8, 9, 15/ and the radial position of the plasma may drift as the fields evolve. In this section these effects will be investigated, together with the resulting evolution of the plasma pressure and B-fields, by using the lowest terms in a series expansion of the equations augmented by global conditions as described at the end of the last section. Estimates are given for the validity of this technique and a representative sample of computer solutions is presented and compared with the corresponding plane slab solutions. The mathematical peculiarities of the infinite cylindrical slab model are discussed in Appendix B.

As before, we assume uniform constant temperature, $n_{\parallel} = C\, n_{\perp}$, and we neglect inertial terms, viscosity and charge separation. We start with Eqs.(1) - (6). However, conditions must be added to these equations to make sure the infinite cylindrical slab approximates a finite height axisymmetric torus. For the axisymmetric torus we may define a flux function $\Psi(r,z,t)$ by

$$B = \nabla \Psi \times \nabla \varphi + B_{\varphi} \hat{\varphi} \tag{39}$$

where φ is the ignorable coordinate angle. Eq. (39) automatically ensures that $\nabla \cdot B = 0$.

Then for solutions of the pressure balance equation $\nabla p = J \times B$ it follows that p and $r B_{\varphi}$ must be uniform over flux surfaces

$$p = p(\Psi,t) \tag{40}$$

$$rB_{\varphi} = f(\Psi,t) \tag{41}$$

In changing to the infinite cylindrical slab, we have changed topology and we must artificially reintroduce these constraints (40) - (41). Without these constraints, a typical solution of Eqs. (1) - (6) would have unequal amounts of poloidal current or poloidal flux flowing up and down in the slab. Note that, while the use of a flux function is a convenience for the axisymmetric torus, it is a necessity for the infinite cylindrical slab.

Now let us change coordinates $(r, \varphi, z) \rightarrow (x, \varphi, z)$ where x is a measure along the radial coordinate from the center of the plasma and is defined by

$$r^2 = r_o^2(t)\,(1 + 2x). \tag{42}$$

Here $r_o(t)$ is adjusted so that Ψ is minimum at $x = 0$. Thus the linear term is missing in the series expansion for Ψ

$$\Psi(x,t) = \Psi_o(t) + \Psi_2(t)x^2 + \Psi_3(t)\,x^3 + \ldots . \tag{43}$$

Note that x corresponds to the inverse aspect ratio which we shall take to be small for our expansions. The slab thickness is approximately $\Delta \sim r_o(t)\ (X_{e+}(t) - X_{e-}(t))$ where $X_{e\pm}(t)$ define the outer or inner edge of the plasma.

In this notation the relevant equations (1) - (6) become

$$B = (\partial\Psi/\partial x)\ /r_o^2\ \hat{Z} + B_\varphi\ \hat{\varphi} \tag{44}$$

$$rJ_\varphi = -\ (1+2x)\ (\partial^2\Psi/\partial x^2)\ /\ r_o^2\ ;\ J_z = \partial f(\Psi)\ /\partial x \tag{45}$$

$$r_o^2\ (1 + 2x)\ p'(\Psi) + f\ f'(\Psi) = rJ_\varphi \tag{46}$$

$$C\ J\ .\ B\ = Sc\ E\ .\ B \tag{47}$$

$$v_r = -\ (\partial p/\partial x)\ /\ SB^2 + cE \times B\ /\ B^2 \tag{48}$$

$$\partial f/\partial t = (1+2x)\partial(c\ E_z)\ /\ \partial\ x \tag{49}$$

$$\partial\Psi/\partial t = -\ rc\ E_\varphi \tag{50}$$

$$\partial p/\partial t = -\ (\partial(p\ rv_r)\ /\ \partial x)\ /\ r_o^2. \tag{51}$$

The last four equations are correct when r_o is fixed. When r_o changes with time, the time derivatives must be modified by

$$\frac{\partial}{\partial t} \rightarrow \frac{\partial}{\partial t} - \frac{\partial}{\partial t}\ (\ell n\ r_o^2(t))\ (1+2x)\ \frac{\partial}{\partial x} \tag{52}$$

and v_r in Eq.(48) refers to the fixed frame.

Eqs.(40) to (51) describe the system we shall study. We shall now outline the formal reduction of these equations to ordinary differential equations before discussing the two new phenomena.

First consider the pressure balance equation. We expand $p(\Psi)$ and $f(\Psi)$ using the form

$$p(\Psi,t) = p_o(t) + p^1(t)\ (\Psi - \Psi_o) + \ldots \ . \tag{53}$$

where the p^1 term is second order in x and it is assumed that the p^2 term is negligible by comparison. Then the lowest two orders of the pressure balance equation (46) are

$$r_o^2 p^1 + f_o f^1 = (rJ_\varphi)_o = -\ 2\ \Psi_2/r_o^2 = -\ B_{z1} \tag{54}$$

$$r_o^2 p^1 \qquad = (rJ_\varphi)_1 = -\ (4\ \Psi_2 + 6\ \Psi_3)/r_o^2 \tag{55}$$

Here, subscripts refer to orders in x. From Ohm's law Eq.(47) we have

$$(rJ_\varphi)_o = Sc(rE_\varphi)_o\ /\ C \tag{56}$$

$$(rJ_\varphi)_1 = r_o^2\ Sc\ E_{zo}\ B_{z1}\ /\ C\ f_o. \tag{57}$$

Note that there must be a uniform verticle E_z-field to support pressure p^1.

The three lowest order evolution equations are

$$\frac{\partial p_o}{\partial t} = \left[2p^1\Psi_2 - Sc\left((rE_\varphi)_o\ B_{z1} - E_{z1}\ f_o\right) + Sc\ E_{zo} f_o\right] p_o/Sf_o^2 \tag{58}$$

$$\frac{\partial \Psi_o}{\partial t} = -\ (rc\ E_\varphi)_o\ , \qquad \frac{\partial f_o}{\partial t} = c\ E_{z1}. \tag{59}$$

The first term in Eq. (58) represents Spitzer diffusion, the middle two terms in parentheses represent the two pinch effects, and the last term represents the Pfirsch-Schlüter effect.

All the equations (40) - (51) have now been used, up to the appropriate order in x.

We find that there are more unknowns than equations and if we go to higher order in the equations there will still be more unknowns than equations. The system will be closed by considering four boundary conditions and one global conservation condition. When applying these conditions, we truncate the expansions [Eqs.(43) and (53)] at the desired order and use the truncated forms out

to the edge of the plasma. For example, here we use a parabolic profile for $\Psi(x)$ and $p(x)$; however, the same method may be used for a higher order truncation.

The boundary conditions are:

1) The pressure is zero at the edge of the plasma. Using the parabolic approximation, which is the lowest order approximation for large aspect ratios,

$$p(x,t) = p_o(t) \ (1 - x^2/ a^2(t)) \tag{60}$$

where $a(t)$ is related to the total thickness $\Delta(t)$ of the plasma

$$\Delta = 2 \ r_o \ a, \tag{61}$$

we find the relation

$$p^1(t) = - p_o(t) \ / \ \Psi_2(t) \ a^2(t). \tag{62}$$

2) The toroidal field, $rB_\varphi = f(\Psi,t)$, is taken to be a fixed constant f_e outside the plasma. Then

$$f^1(t) = (f_e - f_o(t)) \ / \ \Psi_2(t) \ a^2(t). \tag{63}$$

3) The poloidal flux must be continuous across the plasma boundary. Referring to Fig.(5), we find the fluxes at the inner and outer plasma edges are

$$\Psi_- = \tfrac{1}{2} I_{iw} r_{iw}^2 + \tfrac{1}{2} B_2 r_o^2 \ (1 - 2a) \tag{64}$$

$$\Psi_+ = \Psi_{ow} + \tfrac{1}{2} B_4 \ (r_o^2(1+2a) - r_{ow}^2). \tag{65}$$

Here we are defining Ψ as the poloidal flux, through the area between the center line and the given radius, divided by 2π. I_{iw} is the toroidal current per unit height on the inner wall and Ψ_{ow} is the flux at the outer wall. Using the condition that the fluxes must be the same at the inner and outer edges of the plasma, $\Psi_+ = \Psi_-$, we find

$$r_o^2(t) = \frac{1}{2} r_{ow}^2 + (\frac{1}{2} I_{iw} r_{iw}^2 - \Psi_{ow}) / B_4(t) + O(a r_{ow}^2). \quad (66)$$

This equation determines the position of the plasma relative to the walls. In general, Eq. (66) indicates that the plasma will drift to the inner or the outer wall as the poloidal field $B_4(t)$ decays. The simplest field programming we may use to avoid this drift is to fix the current on the inner wall and the flux on the outer wall so that

$$\Psi_{ow} = \frac{1}{2} I_{iw} r_{iw}^2 \quad (67)$$

for the duration of the experiment. This condition fixes the plasma radius at

$$r_o = r_{ow} / \sqrt{2} \quad (68)$$

which, in fact, is close to the operating position used in the present Belt Pinch. More about this later.

4) The poloidal B_z-field must be continuous across the plasma edge. Using the parabolic approximation for the flux within the plasma and Eq. (65) we find

$$\Psi_o(t) = \Psi_{ow} - \Psi_2(t)\ a(t)\ (1 - a(t)). \quad (69)$$

It is convenient to use as a variable the nominal poloidal B_z-field at the edge of the plasma

$$B_{ze}(t) = - 2\ \Psi_2(t)\ a(t) / r_o^2 \quad (70)$$

To lowest order $B_{ze} = B_4 = - B_2$. Then Eq. (69) relates $B_{ze}(t)$ to the flux at the center of the plasma $\Psi_o(t)$.

5) Finally we shall take the amount of plasma per unit height of the cylinder to be a fixed constant.

This implies

$$a(t)\ p_o(t) = N \quad (71)$$

where N is constant.

Alternatively, we could allow for end contraction or for plasma lost to the system by prescribing an evolution for N. This step is planned for future work on two dimensional systems.

After applying these constrants (1) - (5) to the lowest order evolution equations (58) and (59) we find ordinary differential equations for the cylindrical slab which parallel the plane slab equations (31) - (38):

$$\frac{1}{B_{ze}} \frac{d B_{ze}}{d\tau} = W_{bz} = W_{\psi z} - \frac{a}{1-a} W_p \tag{72}$$

$$\frac{1}{p_o} \frac{dp_o}{d\tau} = W_p = W_{sp} + W_{ey} + W_{ez} + W_{p\text{-}sch} \tag{73}$$

Using dimensionless time

$$\tau \equiv t / r_o^2 \, s \tag{74}$$

the decay decrements are, for Spitzer diffusion

$$W_{sp} = - 2 \, p_o / a^2 \, B_{\varphi o}^2 \tag{75}$$

the $E_y \times B_z$ pinch effect

$$W_{ey} = C \, B_{ze}^2 / a^2 \, B_{\varphi o}^2 \tag{76}$$

the $E_z \times B_\varphi$ pinch effect

$$W_{ez} = \left[B_{ze}^2 W_{\psi z} - \left(p_o + \frac{a}{1-a} B_{ze}^2\right) (W_{sp} + W_{ey} + W_{p\text{-}sch})\right] / \left[2 B_{\varphi o}^2 - B_{\varphi o} B_{\varphi e} + Po + aB_{ze}^2 / (1-a)\right] \tag{77}$$

and the Pfirsch-Schlüter effect

$$W_{p\text{-}sch} = - 4 \, C \, p_o / B_{ze}^2. \tag{78}$$

The decay decrement $W_{\psi z}$ is the same that given by Eq. (34).

We have used the notation

$$B_{\varphi o}(\tau) = f_o(\tau) \,/\, r_o$$

$$B_{\varphi e} \quad = f_e \,/\, r_o. \tag{79}$$

Given $B_{ze}(\tau)$ and $p_o(\tau)$ at every time step, we compute $B_{\varphi o}(\tau)$ from the lowest order pressure balance equation (54) written in the form

$$B_{\varphi o}^2 - B_{\varphi e}\, B_{\varphi o} + p_o - B_{ze}^2/2 = 0 \tag{80}$$

and compute $a(\tau)$ from Eq.(71). Hence Eqs. (71) to (80) form a complete system.

Let us consider the conditions under which this system is valid. First of all we have neglected the cubic term in the series expasion of the poloidal flux [Eq.(43)]; $| \, x \, \Psi_3 \, | \ll \Psi_2$. Determining Ψ_2 and Ψ_3 from the lowest two orders of the pressure balance equation [Eqs. (54) and (55)], we find that a small inverse aspect ratio is necessary for this approximation

$$a \ll | \, B_{\varphi o} \, (B_{\varphi e} - B_{\varphi o}) - p_o | / | B_{\varphi o} (B_{\varphi e} - B_{\varphi o}) \, | . \tag{81}$$

Note that the term on the right is generally of order one for low β plasmas.

Secondly, when evaluating the diffusion velocity [Eq. 48] we have approximated $B^2 \simeq B_{\varphi o}^2$. This implies the condition

$$2\, p_o \ll B_{\varphi o}^2. \tag{82}$$

Note that the paramagnetic effect, $B_{\varphi o}^2 > B_{\varphi e}^2$, which is observed when the pinch effect is one of the dominant terms in Eq. (73), strengthens this approximation. The other conditions necessary for the truncation procedure used here have not been evaluated.

Before looking at sample solutions of these equations, let us consider the two new effects that distinguish the cylindrical slab from the plane slab.

It follows from Eq.(66) that the radial position of the plasma is determined by the current on the inner wall, the flux on the outer wall, and the poloidal field $B_4 \simeq B_{ze}$. Suppose the first two are constant in time. If they are adjusted so that the initial position is $r_o = r_{ow} / \sqrt{2}$, then the plasma will stay at this position as B_{ze} decays. However, if the initial position is perturbed in or out, then the plasma will fall in or out as B_{ze} decays. Hence the radial position of the plasma is unstable on the time scale of the decay of the toroidal current. Such behavior has been observed in previous Belt Pinch experiments /33, 35/.

As an alternative boundary condition, suppose the inner wall is a constant flux surface (B_1 fixed) rather than a constant current surface ($I_{iw} = B_1 - B_2$ fixed) as above. Then it can be shown that, even if the initial radial position is $r_o = r_{ow}/\sqrt{2}$ as above, the plasma always falls to the inner wall as B_{ze} decays

$$r_o^2(t) = \frac{1}{2}\left[r_{ow}^2 - r_{iw}^2\,(B_{ze}(o)/B_{ze}(t) - 1)\right]. \qquad (83)$$

Hence, it is preferable to hold the current fixed on the inner wall and not the flux.

We now consider the Pfirsch-Schlüter effect /5, 6, 8, 9, 15/ in the cylindrical slab. From Eqs. (55) and (57) we see that the equilibrium requires a vertical electric field. In the presence of the toroidal B-field, this electric field induces a zero order radial flow directed away from the center line of the cylinder

$$(rv_r)_o = 4\,C\,p_o/S\,B_{ze}^2. \qquad (84)$$

The time it takes for a given element of plasma to cross the slab of thickness Δ

$$\tau_\Delta \sim \Delta\, r_o\, S\, B_{ze}^2 \,/\, 2\, p_o. \tag{85}$$

If the position of the slab as a whole is fixed, the plasma must return by flowing along the field lines and around the ends of the slab /6/. The centrifugal force of this flow has little effect on the equilibrium if

$$\frac{M_i\, V_i^2}{T_e}\,\frac{h}{R} \sim \frac{.36}{T_e^{\,4}[ev]}\,\frac{1}{\iota^4}\left(\frac{\beta_\varphi}{a}\,\frac{2\, r_o}{h}\right)^2 \frac{h}{R} \ll 1$$

where R is the maximum radius of curvature of the field line ($\leqslant r_o$), h is the height of the plasma ($\sim 2\, r_o$), ι is the rotational transform [see Eq. (87)], $\beta_\varphi = 2\, p_o / B_{\varphi e}^2$ and a, given by Eq. (61), are dimensionless forms.

High temperatures and moderate values of rotational transform are needed to make this effect negligible.

The net plasma loss across the flux surfaces due to the Pfirsch-Schlüter effect, as indicated in Eq. (78), results from the fact that the first (and higher) order flow is not divergence free. Comparison of the decay decrements (75) and (78) shows that the Pfirsch-Schlüter effect becomes important only when

$$B_{ze}^2 \leqslant a^2\, B_{\varphi o}^2. \tag{86}$$

For the Belt Pinch, this is generally true only late in the discharge. For highly elongated cross sections, the rotational transform is approximately

$$\iota \simeq \frac{2\, r_o}{h}\left|\frac{B_{ze}}{B_{\varphi o}}\right| \tag{87}$$

where h is the height of the plasma cylinder. In the present Belt Pinch the height of the plasma is roughly the same as the diameter, $h \sim 2\, r_o$, although it varies during the discharge. Thus the condition for the dominance of the Pfirsch-Schlüter effect [Eq.(86)] becomes $\iota \leq a$. In the experiment, the maximum value of ι is kept just below 1, the Kruskal-Shafranov stability condition, and the plasma is initially made thin, $a \ll 1$. Therefore the Pfirsch-Schlüter effect becomes dominant only late in the discharge after ι has decayed and the plasma has spread out in thickness.

Figures (6a - 8a) (solid curves) show the evolution of $B_{ze}(t)$, $p_o(t)$, and $a(t)$ for a cylindrical slab and figures (6b - 8b) show the corresponding decay decrements [Eqs. (75) - (78)]. The normalization $B_{\varphi e} = 1$ is used throughout. The initial values $p_o(o) = .2$ and $a(o) = .02$ are the same for all three graphs while the initial values $B_{ze}(o) = 1.$, .3, and .1 are chosen for succeeding graphs. B_{ze} is approximately the rotational transform ι if the plasma height equals the plasma diameter [Eq. 87]. The vertical scales are logarithmic while the horizontal scale is linear in the dimensionless time $\tau \equiv t/r_o^2 S$. For $T_e = 10$ eV and $r_o = 22.6$ cm the full time range shown is 250 μsec; the decay time scale for B_{ze} in Fig. (6a) is less than 50 μsec which roughly agrees with present experimental observations. In the next generation Belt Pinch we expect $r_o = 53$ cm; then for $T_e = 100$ eV the full time range shown is 43.5 msec.

One sees immediately that for $B_{ze} \sim O(1)$ the pinch effect $E_y \times B_z$ is an important but transient effect.

Increasing the initial plasma thickness, a(t=o), does not change this effect but it lengthens the time scales. Decreasing the initial pressure of course increases this pinch effect but it remains a transient. The other pinch effect, $E_z \times B_\varphi$, is always negligible for these moderate to low values of $\beta \leq .4$.

The Pfirsch-Schlüter effect dominates later in the discharge (see $W_{p\text{-}sch}$ in Figs. (6b - 8b)) after the pinch effect is negligible. At first the Pfirsch-Schlüter decay decrement, $W_{p\text{-}sch}$, decreases in Figs. (7b) and (8b) because $p_o(t)$ initially decays faster than $B_{ze}{}^2(t)$; but then $W_{p\text{-}sch}$ levels off when $p_o(t)$ and $B_{ze}{}^2(t)$ decay at comparable rates.

Figures (6) - (8) apply to a Belt Pinch with fixed height, provided no plasma is lost and end effects or force-free-fields have negligible effect. Figure (9) illustrates the opposite extreme where the thickness of the plasma, a, is fixed (a =.0 2 here) and the height varies like $1/p_o$ in order to conserve the total amount of plasma. Fig.(9) should be compared with the cylindrical slab part of Fig. (6). The transient pinch effect is roughly the same. The poloidal field $B_{ze}(t)$ decays at a constant rate because a is fixed (and the second term in Eq.(72), which follwed from da/dt, is zero). With fixed a, Spitzer diffusion follows a $1/t$ behavior rather than a $t^{-1/3}$ behavior. Hence the central pressure p_o drops more rapidly. The diffusion time scales remain closer to their initially fast values, by comparison to the expanding plasma case, so that the Pfirsch-Schlüter effect rises to dominance sooner.

Clearly, more must me learned about the Belt Pinch equilibrium in order to determine the evolution of the plasma height (or thickness) together with the evolution of the pressure and fields.

Conclusions

The following typical sequence of events take place during the classical diffusion of a uniform temperature free boundary plasma slab.

For an initially high-β plasma there is a rapid decay of the poloidal electric field. Then the pressure profile decays to a nearly parabolic shape. These are estimated to be transients on the diffusion time scale.

If there are sufficiently large poloidal fields the plasma may be compressed through a succession of equilibria. However, this pinch effect rapidly gives way to Spitzer diffusion which imparts an algebraic time dependence to the central plasma pressure $p_o(t)$ while the poloidal B-field decays more exponentially on a longer time scale. Later in the discharge, the Pfirsch-Schlüter effect dominates in the pressure decay.

There is an open question concerning how this picture is altered by the evolution of the plasma height or the plasma shape. To answer this question one must know how the externally applied fields determine the shape of the equilibrium. Also, it would be useful to have a simple model to predict the overall temperature of the plasma and at least the general features of the temperature profile.

However, the detailed analysis of the simple model presented here provides some basic understanding of the relation between the various forms of diffusion as well as a tool for making rough estimates of the behavior of the Belt Pinch plasma.

Appendix A

The following are a list of numerical estimates of various terms in the moment equations. These estimates may be used to justify the neglect of inertial effects, viscosity, and charge separation for the diffusion problems considered in this paper. That is, we justify using Eqs. (1) - (6)) as a good approximation to the full moment equations.

The moment equations, as written by Braginskii /26/, are derived under the condition that the electrons undergo many Larmor gyrations during a collision time

$$\omega_e \tau_e \sim 20 \left(\frac{B}{10\ kG} \right) \left(\frac{T_e}{10\ ev} \right)^{3/2} \left(\frac{10^{16}}{n_e} \right) \gg 1 \qquad \text{(A-1)}$$

Either high temperature or low density is needed to ensure this approximation.

In order to write the moment equations and Maxwell's equations in the same variables, the velocities of the individual species are transformed to current density, $j \equiv c\ J/\ 4\pi$, and fluid velocity, v. To simplify this transformation we neglect the mass ratio, $Z_i\ m_e/m_i$ and the charge separation characterized by the dimensionless form $(n_i Z_i - n_e)/\ n_e$. For an estimate of the charge separation between the center and the edge of the plasma, we estimate the electric field induced by the Hall effect

$$E_\perp \sim T_e/\ e\ \Delta \qquad \text{(A-2)}$$

for a slab of thickness Δ. We then estimate the resulting charge separation from Maxwell's equations

$$(n_i Z_i - n_e)\ /\ n_e \sim \lambda_{De}^{\ 2}/\Delta^2 = 5.53 \times 10^5 \frac{T_e[ev]}{n_e[1/cm^3]\,\Delta^2[cm]} \ll 1. \qquad \text{(A-3)}$$

This charge separation can be neglected whenever the Debye length is much smaller than the plasma thickness.

Now consider the resulting moment equations on the shortest possible diffusion time scale

$$\tau = \Delta^2 S = .124\ T_e^{3/2}[ev]\ \Delta^2[cm]\ \mu sec. \qquad (A-4)$$

Then an estimate for the maximum Spitzer diffusion velocity follows from the equation of continuity

$$v \sim \Delta/\tau. \qquad (A-5)$$

The Pfirsch-Schlüter flow velocity [Eq. (84)] may be entirely different so that a separate estimate is made for the inertial effects due to that flow [Eq. (85)].

From the sum of the momentum conservation equations in plane slab geometry we find

$$m_i\ n_i\ dv_i/dt + \nabla p - J \times B - \sigma E - .32 \frac{\partial}{\partial x}\left(n_i\ T_i\ \tau_i \frac{\partial v}{\partial x}\right) = 0 \qquad (A-6)$$

where Braginskii's article /26/ may be referred to for notation (except that $j = c\ J/4\pi$). After rendering this equation dimensionless, we find that the inertial term may be neglected when

$$m_i\ v^2/T_i = \frac{68.\ (m_i/m_p)}{T_e^3\ T_i[ev]\ \Delta^2[cm]} \ll 1; \qquad (A-7)$$

the term σE may be neglected when

$$v^2/\beta\ c^2 = \frac{7.24 \times 10^{-8}}{\beta\ T_e^3[ev]\ \Delta^2[cm]} \ll 1\ ; \qquad (A-8)$$

and the viscosity term (last term) may be neglected for a Deuterium plasma when

$$\tau_i/\tau \sim 1.7 \times 10^{-3} \left(\frac{10^{16}}{n_e}\right) \left(\frac{1\ cm}{\Delta}\right)^2 \ll 1. \qquad (A-9)$$

We are then left with the pressure balance equation, $\nabla p = J \times B$.

From the appropriate difference of momentum conservation equations we have (using $C = n_\parallel/n_\perp = 1$ for simplicity here)

$$\frac{d}{dt}\left(c^2 J/\omega_p^2\right) = c E - J/S + (v - c J/4\pi e n) \times B$$
$$+ c \nabla (n_e T_e)/e n_e + .32 \frac{c}{e n_e} \frac{\partial}{\partial x}\left(n_i T_i \tau_i \frac{\partial v}{\partial x}\right) \qquad \text{(A-10)}$$

Again using a dimensionless form, the term on the far left scales like

$$c^2/\omega_p^2 \Delta^2 = 2.8 \times 10^{-5} \left(\frac{10^{16}}{n_e}\right) \left(\frac{1 \text{ cm}}{\Delta}\right)^2 \ll 1 \qquad \text{(A-11)}$$

and, relative to the rest of the equation , the viscosity term on the far right scales like

$$\beta \omega_e \tau_e \tau_i/\tau = 3.4 \times 10^{-2} \beta \left(\frac{10^{16}}{n_e}\right)^2 \left(\frac{T_e}{10 \text{ ev}}\right)^{3/2} \left(\frac{1 \text{ cm}}{\Delta}\right)^2 \ll 1.$$

The J x B and $\nabla(n_e T_e)$ terms have no effect on those components of the E-field within the flux surfaces and, when uniform temperature is assumed, they have no effect on Faraday's law $\partial B/\partial t = - \nabla \times cE$.

Appendix B

Infinite Cylindrical Slab as the Limit of a Torus

The infinite cylindrical slab is a useful model because it is the closest one-dimensional approximation to an axisymmetric torus with highly elongated cross section such as the Belt Pinch. Also, it turns out that the diffusion equation is insensitive to this approximation; this can be seen by writing Eq.(73) using the rotational transform [Eq. (87)] as a variable and comparing with Maschke's results for a torus with elliptical cross section / 9 / . However, mathematically, the slab is a singular limit of plasma geometries with finite height. Here, the differences between slab and finite geometries will be catalogued. First among these, a theorem will be proved showing that the solubility condition for the pressure balance equation is different in the two cases.

The pressure balance equation $\nabla p = J \times B$ for an axisymmetric torus may be written

$$\nabla^* \Psi + f f'(\Psi) + r^2 p'(\Psi) = 0 \qquad \text{(B-1)}$$

$$\nabla^* \Psi \equiv \frac{\partial^2 \Psi}{\partial r^2} - \frac{1}{r}\frac{\partial \Psi}{\partial r} + \frac{\partial^2 \Psi}{\partial z^2} \qquad \text{(B-2)}$$

$$\equiv \sigma(r,z)$$

where $\sigma(r,z)$ is related to the toroidal current $\sigma = - r j_\varphi$. It is well known / 36, 37 / that given smooth functions $p(\Psi)$ and $f(\Psi)$ equations generally have one or more solutions for $\Psi(r,z)$ or the corresponding $\sigma(r,z)$. However:

Theorem

Given $\Psi(r,z)$ with a simple mini-max point, or given the corresponding $\sigma(r,z)$, in general there exists no solution of (B-1) for $p(\Psi)$ and $f(\Psi)$.

Proof

Eq. (B-1) actually represents two equations in the variables Ψ and z because $r(\Psi,z)$ is not a single valued function. Let $r = r_{\pm}(\Psi,z)$ on the + or - side of the mini-max of $\Psi(r.z)$. Then Eq.(B-1) becomes the two equations

$$\Sigma_{\pm}(\Psi,z) + f\, f'(\Psi) + r^2_{\pm}(\Psi,z)\, p'(\Psi) = 0 \qquad \text{(B-3)}$$

where

$$\Sigma_{\pm}(\Psi,z) \equiv \sigma\,(r_{\pm}(\Psi,z),\, z). \qquad \text{(B-4)}$$

If $r_+^2(\Psi,z) \neq r_-^2(\Psi,z)$, Eqs.(B-3) can be solved uniquely for $p'(\Psi)$ and $f\, f'(\Psi)$

$$\left.\begin{aligned} p'(\Psi) &= \left[\, \Sigma_-(\Psi,z) - \Sigma_+(\Psi,z) \,\right] / \Delta\,(\Psi,z) \\ f\, f'(\Psi) &= \left[\, \Sigma_+(\Psi,z)\, r_-^2\,(\Psi,z) - \Sigma_-(\Psi,z)\, r_+^2(\Psi,z)\right] / \Delta(\Psi,z) \end{aligned}\right\} \qquad \text{(B-5)}$$

where $\Delta(\Psi,z) \equiv r_+^2\,(\Psi,z) - r_-^2\,(\Psi,z)$

Giving $\Psi = \Psi(r,z)$ completely determines the functions $r_{\pm}(\Psi,z)$ and $\Sigma_{\pm}(\Psi,z)$ so that there is no freedom to make the right hand sides of Eq. (B-5) a function of Ψ alone. Therefore, no solution exists to the pressure balance equation (B-3), in general.

Corollary

For the infinite cylindrical slab, given $\Psi(r)$ with a simple mini-max point or given the corresponding $\sigma(r)$, in general a solution of Eqs. (B-1), (B-3), or (B-5) exists and both $p(\Psi)$ and $f(\Psi)$ are uniquely determined.

For the finite axisymmetric torus the theorem may be paraphased by the statement that the set of functions $\Psi(r,z)$ that are solutions of the pressure balance equation (B-1) is much smaller than the set of all possible functions $\Psi(r,z)$ possessing a simple mini-max. In order to solve the pressure balance equation, one must give $(p(\Psi), f(\Psi))$ and solve for $\Psi(r,z)$ and $\sigma(r,z)$. Alternatively, for the infinite cylindrical slab, the function $\Psi(r)$ can be given, but then $p(\Psi)$ and $f(\Psi)$ are no longer independent functions. The pressure balance equation drastically changes character with the change in topology.

These theorems also illustrate that the pressure balance equation provides a very peculiar constraint for the diffusion equations (1) - (6). We may not think of Ohm's law as determing the toroidal current distribution which in turn determines the pressure profile and poloidal current profile. For an iteration scheme we must solve the equations in reverse and use Ohm's law to determine the velocity flow field. This property of the equations makes 2-D computer solutions of Eqs. (1) - (6) very difficult.

Several more differences between the slab model and the finite model will now be listed.

The "magnetic axis" in the slab model is a sheet whereas, in all the known axisymmetric torus equilibrium solutions, it is one or more lines. Is it possible for the magnetic axis to be a sheet of finite height? Apparently not if Ψ is an analytic function of r and z; i.e. if Ψ is constant along a line in the (r,z)-plane, the line must close on itself or extend to infinity. However, one may have any number of magnetic axes along a line so that one should be able to approximate a "sheet magnetic axis" arbitrarily closely. If it is possible to construct such equilibria, the slab model may be a better approximation to them than the single magnetic axis models which have been investigated before.

Acknowledgements

This work has greatly benefited from frequent dialogues with Professor H. Zwicker and with Dr. W. Grossmann.

Many additional suggestions came from Dr. R. Wilhelm, H. Krause, K. Lackner and the continually evolving Belt Pinch-group.

It is a pleasure to acknowledge the hospitality of Professor E. Fünfer and the high-beta division at the Max-Planck-Institut für Plasmaphysik.

References

/1/ Kruskal,M.D.; Princeton Report PM-S-17 NYO 7307 (1955)

/2/ Kruskal,M.D. and R.M.Kulsrud, Phys.Fluids 1, 265 (1958)

/3/ Rosenbluth,M.N. and A.N.Kaufman, Phys.Rev. 109, 1 (1958)

/4/ Rosenbluth,M.N.; Proc. 2nd Int.Conf.on Peaceful Uses of Atomic Energy, Geneva, Vol. 31, 85 (1958)

/5/ Pfirsch,D. and A.Schlüter, MPI-Report PA/7/62 (1962)

/6/ Shafranov,V.D.;Reviews of Plasma Physics Vol.2, 141 (1963)

/7/ Knorr,G., Phys.Fluids 8, 1334 (1965)

/8/ Kadomtsev, B.B. and V.D.Shafranov; Doklady Akad. Nauk SSSR, 167, 1273 (1966) [Sov.Phys.Doklady 11, 341 (1966)

/9/ Maschke,E.K.; Plasma Physics 13, 905 (1971)

/10/ Johnson,J.L. and S.von Goeler; Phys.Fluids 12, 255 (1969)

/11/ Grad,H. and J.Hogan; Phys.Rev.Lett. 24, 1337 (1970)

/12/ Grad,H.; (private communication), (July 1970)

/13/ Grad,H.; New York Univ. Report NYO-1480-184 (1971)

/14/ Nührenberg,J.; Nuclear Fusion 12, 157 (1972)

/15/ Nührenberg,J.; Nuclear Fusion 12, 383 (1972)

/16/ Green,B.J.; Nuclear Fusion 12, 475 (1972)

/17/ Maschke,E.K. and J.P.Sudano, Fontenay-aux-Roses, Report EUR-CEA-FC-668 (1972)

/18/ Wilhelm,R. and H.Zwicker, 4th Conf. Proceedings, Madison, IAEA-CN-28/B-7 (1971);
Zwicker,H.; Atomkernenergie 19, 184 (1972)
Grossmann,W., H.Krause, R.Wilhelm, H.Zwicker, 2nd Topical Conf. on Pulsed High-Beta Plasmas, Garching, IPP 1/127 (1972)

/19/ Lackner,K. and K.U.von Hagenow (private communication), (1973)

/20/ Ochem,W.; (private communication), (1973)

/21/ Artzimovich,L.A.; Controlled Thermonuclear Reactions (1961) pp 49-60
Galushkin,Yu.L. and V.I.Gervids, V.I.Kogan; 4th Conf. Proceedings, Madison, IAEA/CN-28/F-6 (1971)

/22/ Engelhardt,W.; (private communication), (1973)

/23/ Lotz,W.; IPP 1/62 (1967)

/24/ Krause,H.; (private communication), (1973)

/25/ Strauss,H.R.; Phys.Rev.Lett. 29, 462 (1972)

/26/ Braginskii,S.I.; Transport Processes in a Plasma; in Reviews of Plasma Physics, ed. by M.A.Leontovich (Consultants Bureau N.Y. 1965) Vol.1, 205-219;

/27/ Blank,A.A., K.O.Friedrichs and H.Grad,New York Univ., Report NYO-6486-V(1957);

/28/ Hobbs,G.D.; Culham Reports CLM-R-15 (1961) and CLM-M 22 (1963);

/29/ Holladay,J.; Los Alamos report LA-1962 (1955)

/30/ Bezbachenko, A.L. et al.; Atomnaya Energiya 1, 26 (1956)

/31/ Bickerton,R.J.; Proc. Phys. Soc. B 72, 618 (1958)

/32/ Belitz,H.J., et al. 4th Conf.Proceedings, Madison, IAEA-CN-28/J-2;

/33/ Schlüter,J.; (private communication), (1972)

/34/ Biot,M.A.; Variational Principles in Heat Transfer, Oxford Clarendon Press (1970)

/35/ Wilhelm,R. and H.Krause (private communication), (1972)

/36/ Marder,M.B. and H.Weitzner, Plasma Phys. 12, 435 (1970)

/37/ Anderson,D.V., J.Killeen and M.E.Rensink, Phys. Fluids, 15, 351 (1972)

Figure captions

Fig. 1 Cooling rate due to 1 % Oxygen impurity in various ionization stages (Corona model /22/) and Ohmic heating rate for slab of thickness Δ carrying uniform volume current.

Fig. 2 Notation and conventions for the plane slab model.

Fig. 3 Plane slab similarity solutions [Eqs.(21) and (23)] for Spitzer diffusion; illustrating the difference between algebraic pressure decay and exponential B-field decay.

Fig. 4 Plane slab limit profiles (normalized). Solid curves for $\beta = .9$, dashed curves for $\beta \to 0.$ and $\beta \to 1.$

Fig. 5 Notation and conventions for cylindrical slab model.

Fig. 6 Time-dependent diffusion for plane and cylindrical slabs with fixed height. Normalization: $B_{\varphi e} = 1.$ Dimensonless time scale: $t/S\ r_o^2$. Initially $B_{ze} = 1.$, $p_o = .2$, $a = .02$. Note initial pinch effect and late Pfirsch-Schlüter effect.

Fig. 7 Time-dependent diffusion for plane and cylindrical slabs with fixed height. Initially $B_{ze} = .3$, $p_o = .2$, $a = .02$.

Fig. 8 Time-dependent diffusion for plane and cylindrical slabs with fixed height. Initially $B_{ze} = .1$, $p_o = .2$, $a = .02$. Cylindrical calculation ends when $a = .3$.

Fig. 9 Time-dependent diffusion for plane slab with fixed thickness $a = .02$ and variable height (not shown). Initially $B_{ze} = 1.$ and $p_o = .2$.

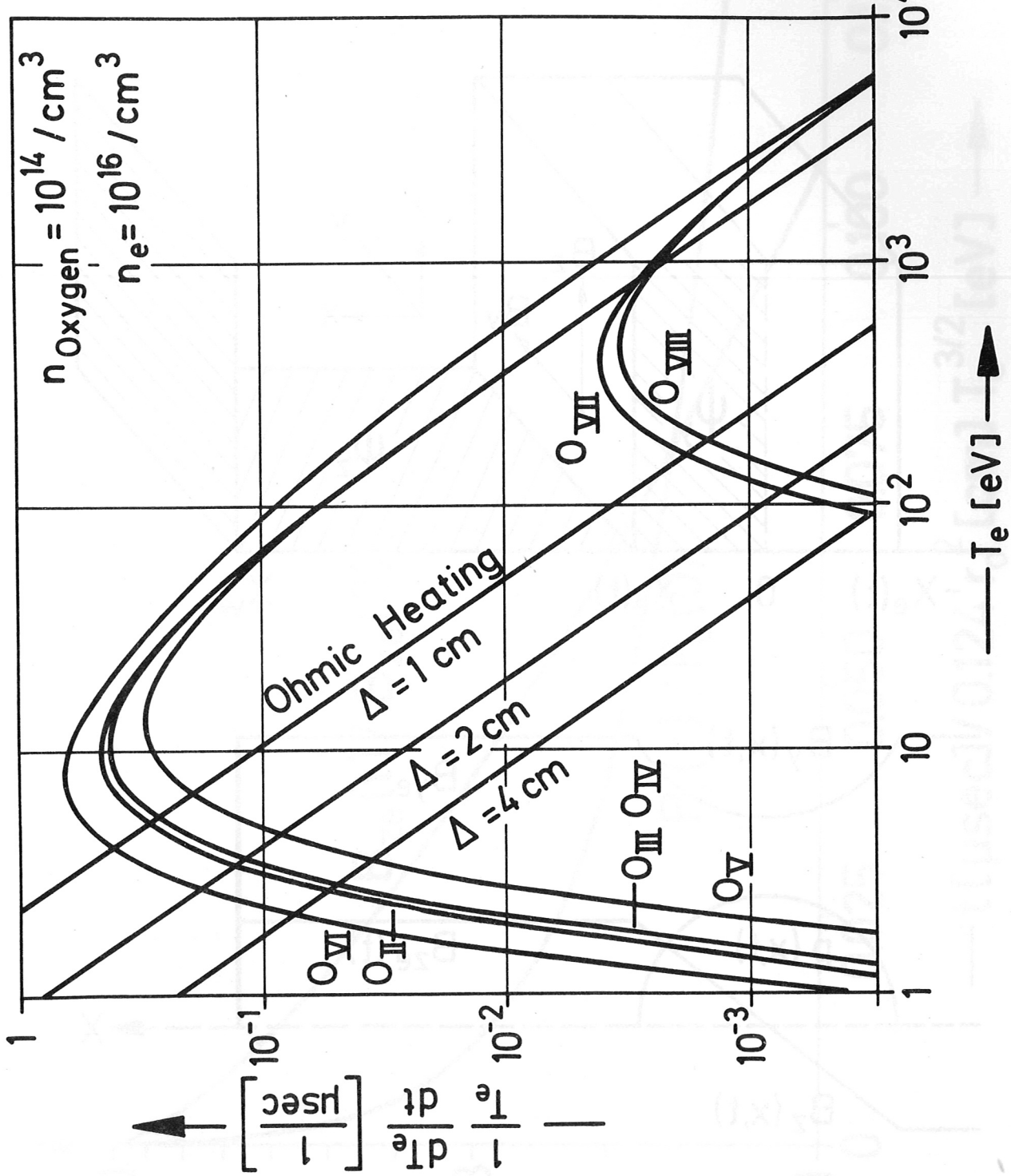
$n_{Oxygen} = 10^{14}/cm^3$
$n_e = 10^{16}/cm^3$
Ohmic Heating
Δ = 1 cm
Δ = 2 cm
Δ = 4 cm
O VII
O VIII
O III
O IV
O V
O II
O I
$\frac{1}{T_e}\frac{dT_e}{dt}\left[\frac{1}{\mu sec}\right]$
T_e [eV]
1
10^{-1}
10^{-2}
10^{-3}
10
10^2
10^3
10^4

Fig. 1

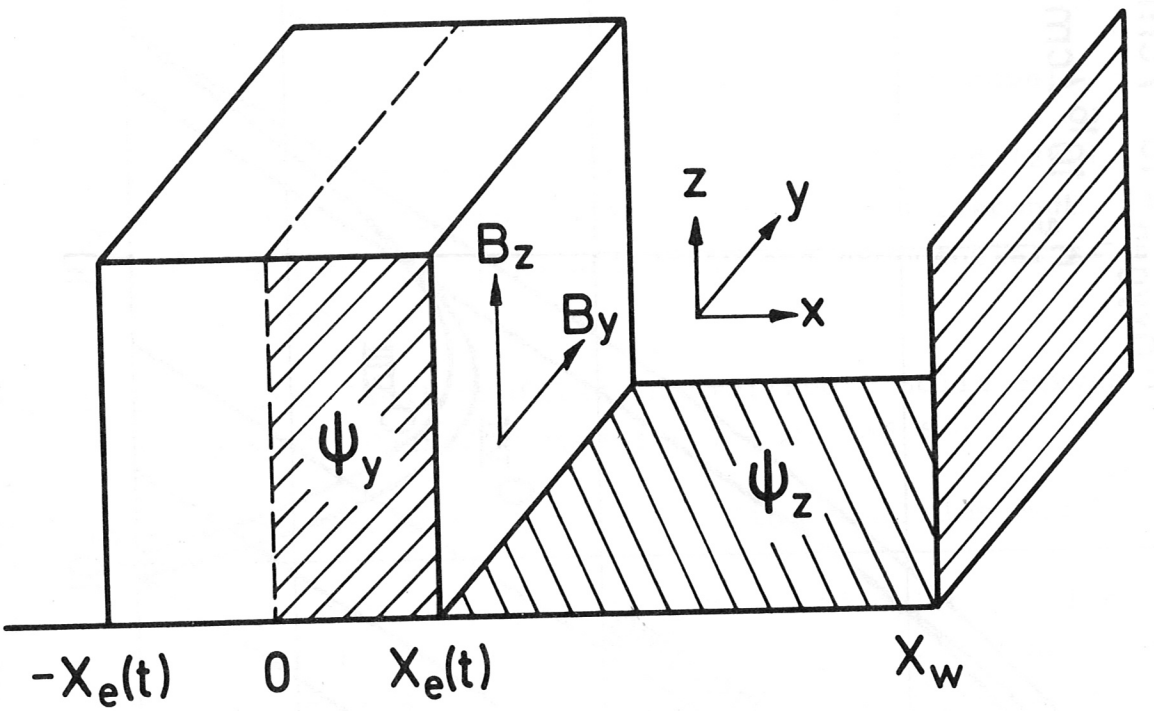

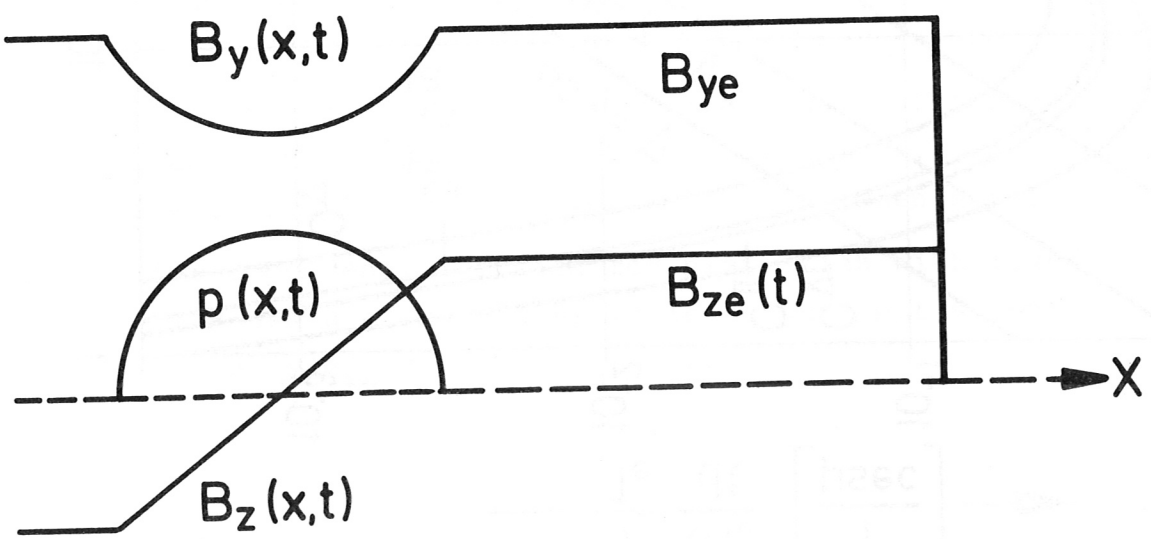

Fig. 2

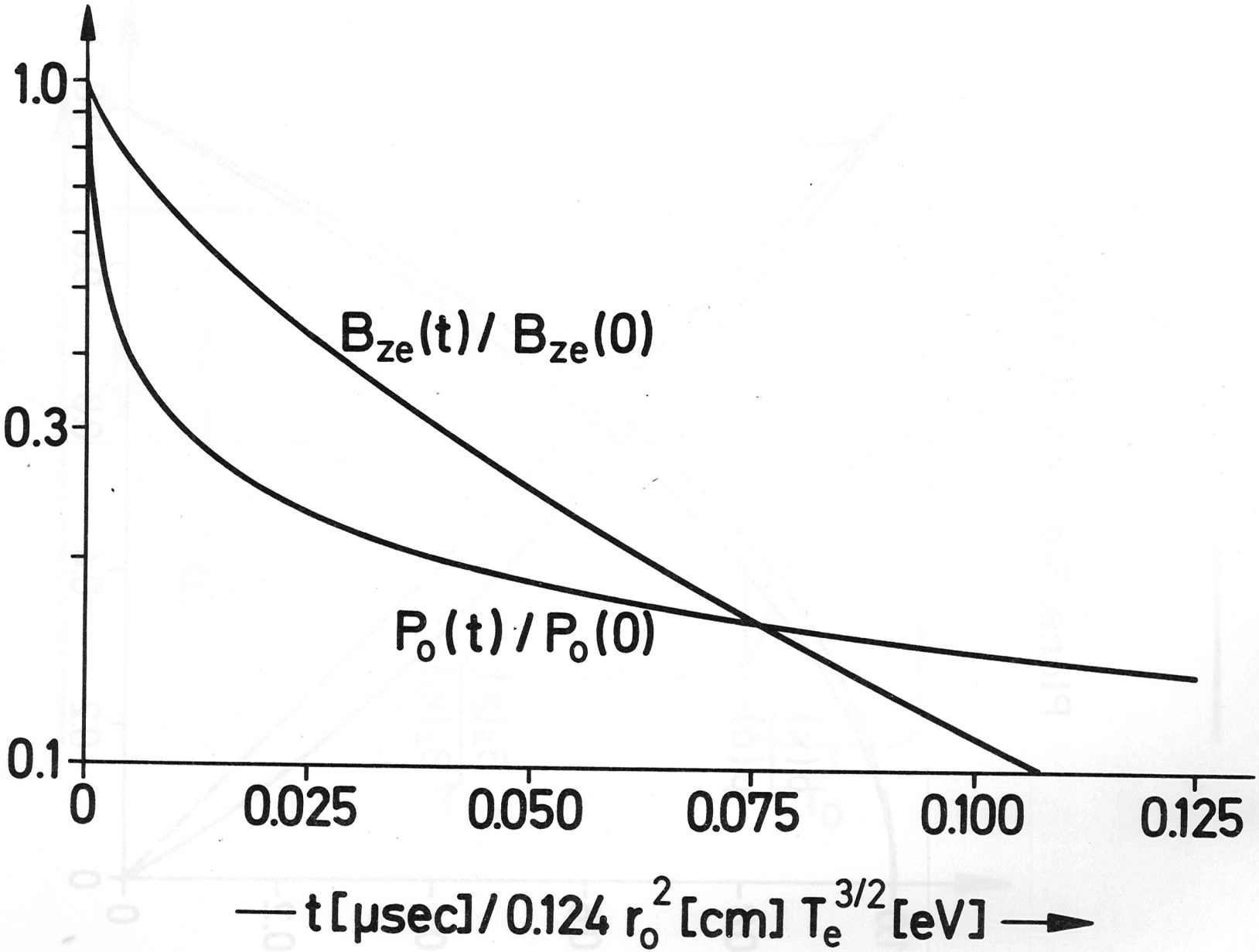
1.0
0.3
0.1
$B_{ze}(t) / B_{ze}(0)$
$P_o(t) / P_o(0)$
0
0.025
0.050
0.075
0.100
0.125
— t [μsec] / 0.124 r_o^2 [cm] $T_e^{3/2}$ [eV] →

Fig. 3

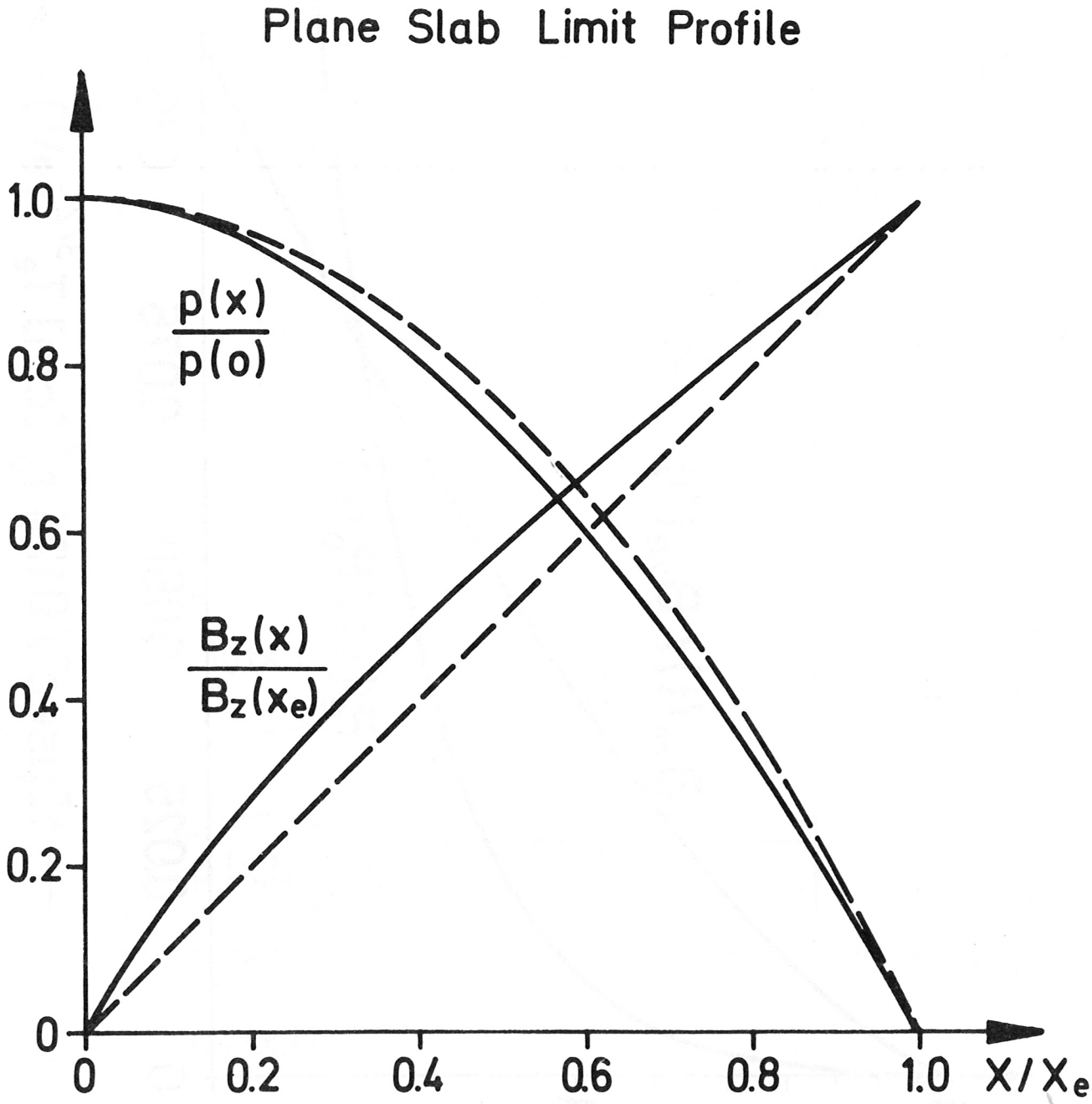
Plane Slab Limit Profile
1.0
0.8
0.6
0.4
0.2
0
p(x)/p(o)
Bz(x)/Bz(xe)
0
0.2
0.4
0.6
0.8
1.0
X/Xe

Fig. 4

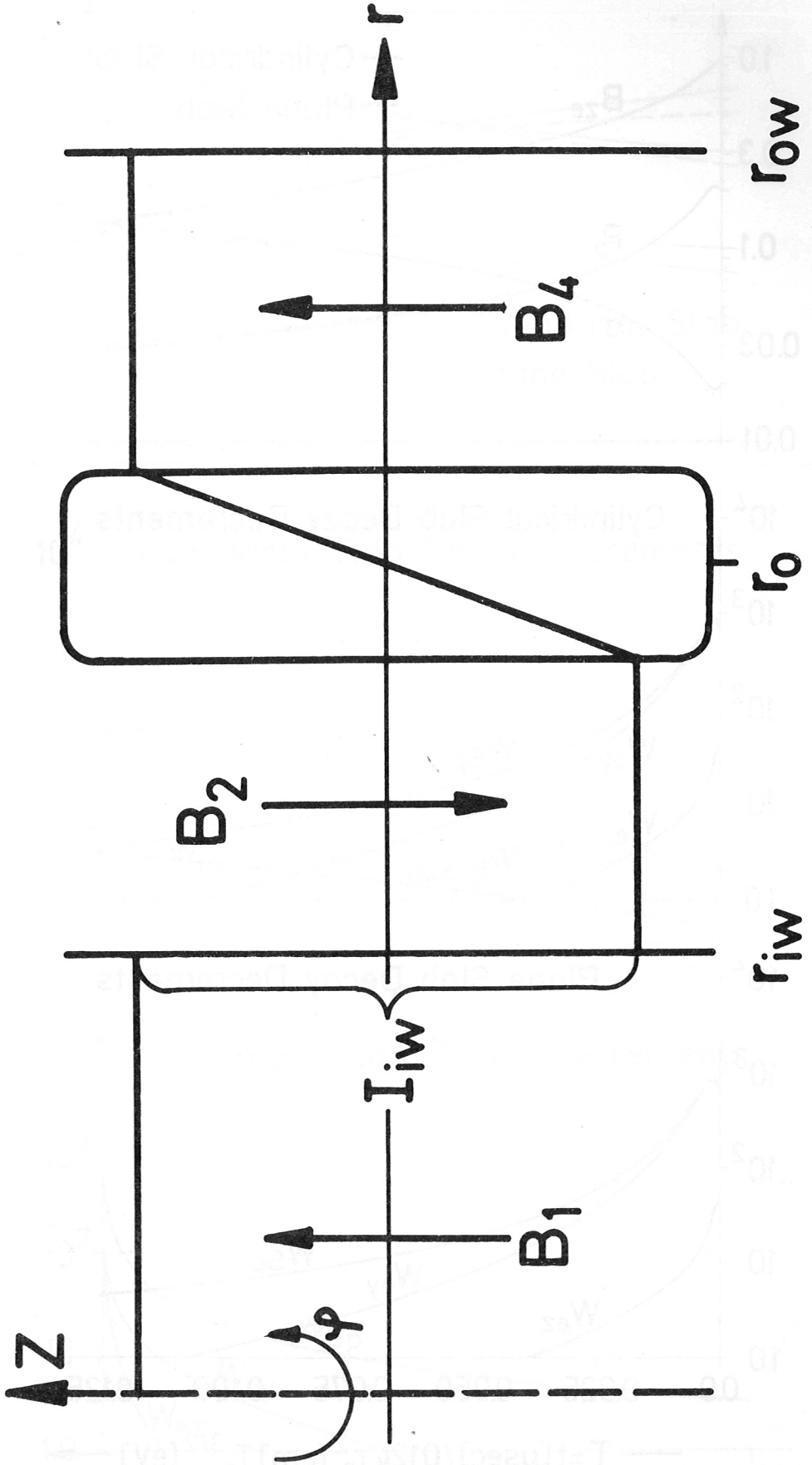

Fig. 5

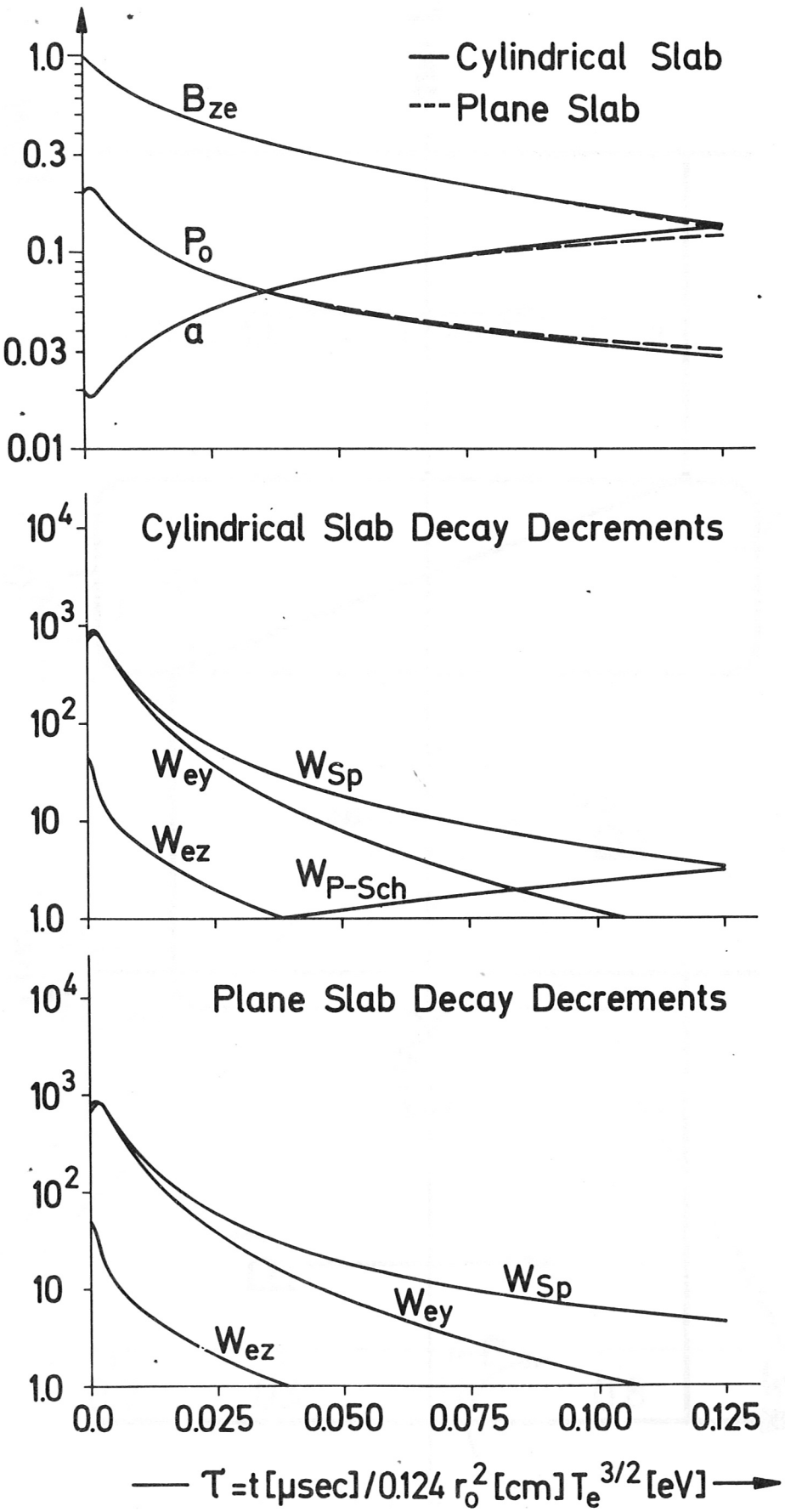
1.0
0.3
0.1
0.03
0.01
Bze
Po
a
Cylindrical Slab
Plane Slab
Cylindrical Slab Decay Decrements
10^4
10^3
10^2
10
1.0
Wey
Wez
WSp
WP-Sch
Plane Slab Decay Decrements
10^4
10^3
10^2
10
1.0
WSp
Wey
Wez
0.0
0.025
0.050
0.075
0.100
0.125
T = t [μsec] / 0.124 r0^2 [cm] Te^3/2 [eV]

Fig. 6

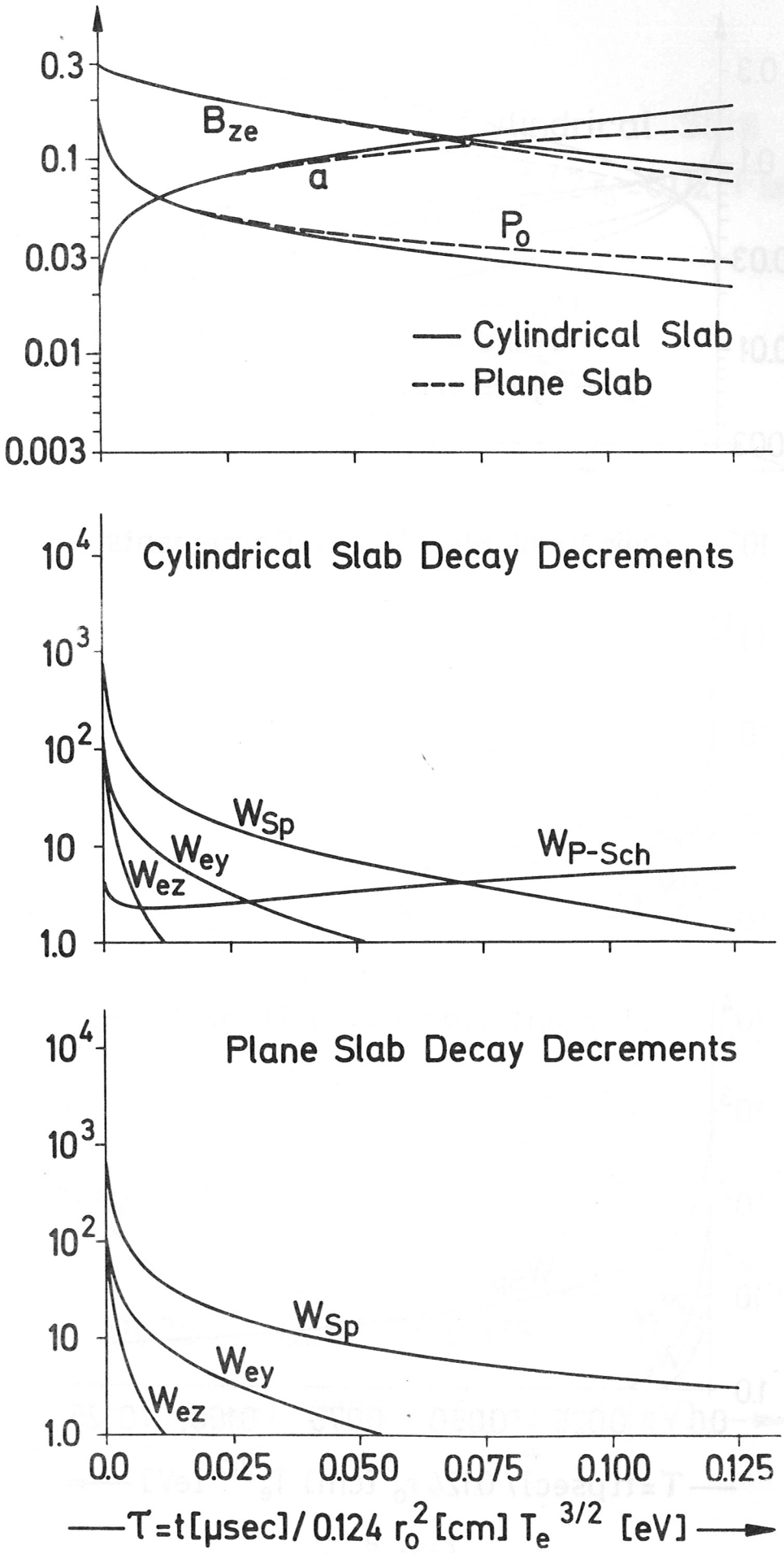
0.3
0.1
0.03
0.01
0.003
B_{ze}
a
P_o
Cylindrical Slab
Plane Slab
10^4
10^3
10^2
10
1.0
Cylindrical Slab Decay Decrements
W_{Sp}
W_{ey}
W_{ez}
$W_{P\text{-}Sch}$
10^4
10^3
10^2
10
1.0
Plane Slab Decay Decrements
W_{Sp}
W_{ey}
W_{ez}
0.0
0.025
0.050
0.075
0.100
0.125
$\tau = t[\mu sec] / 0.124\ r_o^2[cm]\ T_e^{3/2}[eV]$

Fig. 7

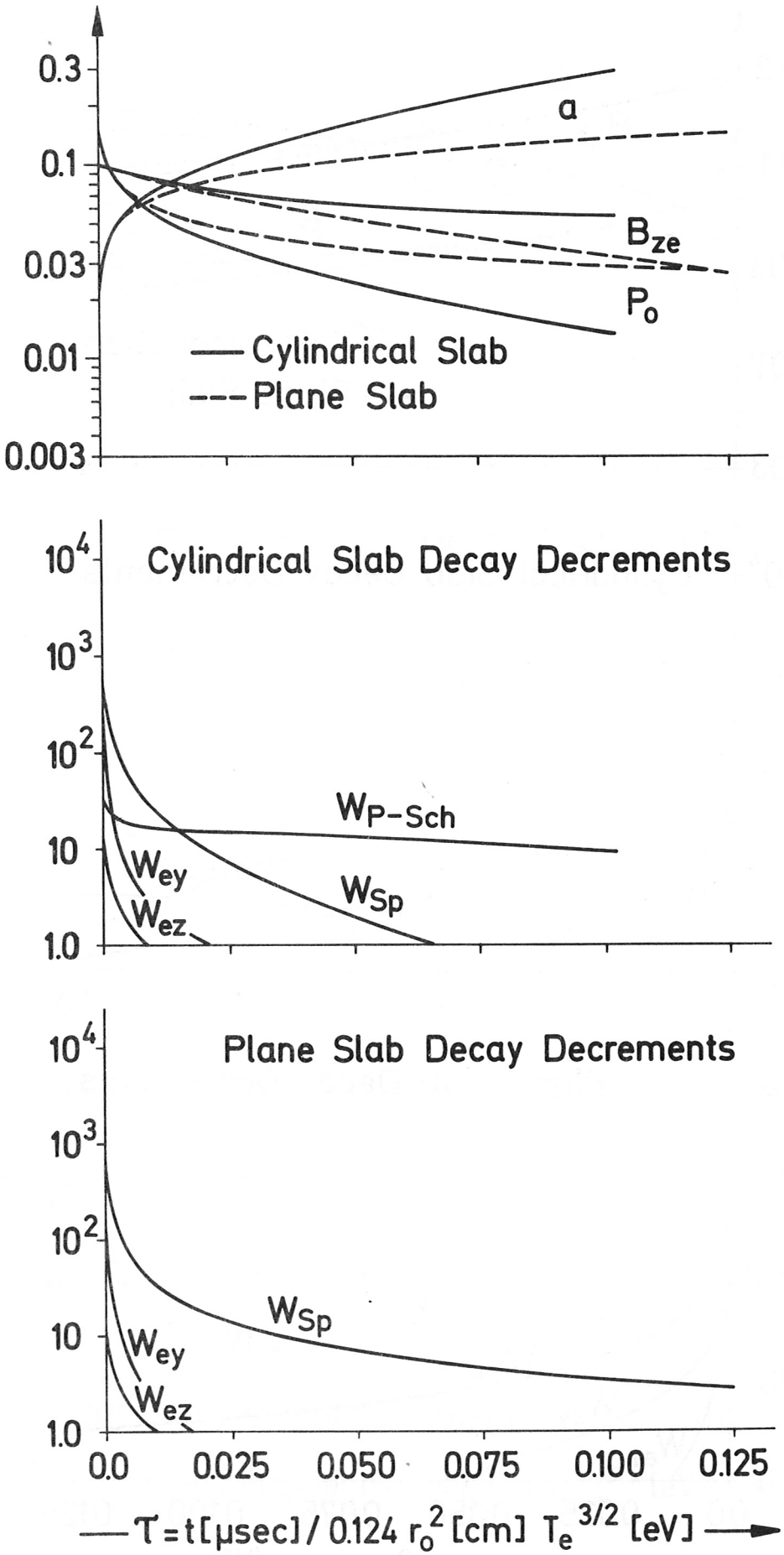
0.3
0.1
0.03
0.01
0.003
a
B_{ze}
P_o
Cylindrical Slab
Plane Slab
10^4
10^3
10^2
10
1.0
Cylindrical Slab Decay Decrements
W_{P-Sch}
W_{ey}
W_{ez}
W_{Sp}
Plane Slab Decay Decrements
0.0
0.025
0.050
0.075
0.100
0.125
$\tau = t[\mu sec] / 0.124\, r_o^2\,[cm]\, T_e^{3/2}\,[eV]$

Fig. 8

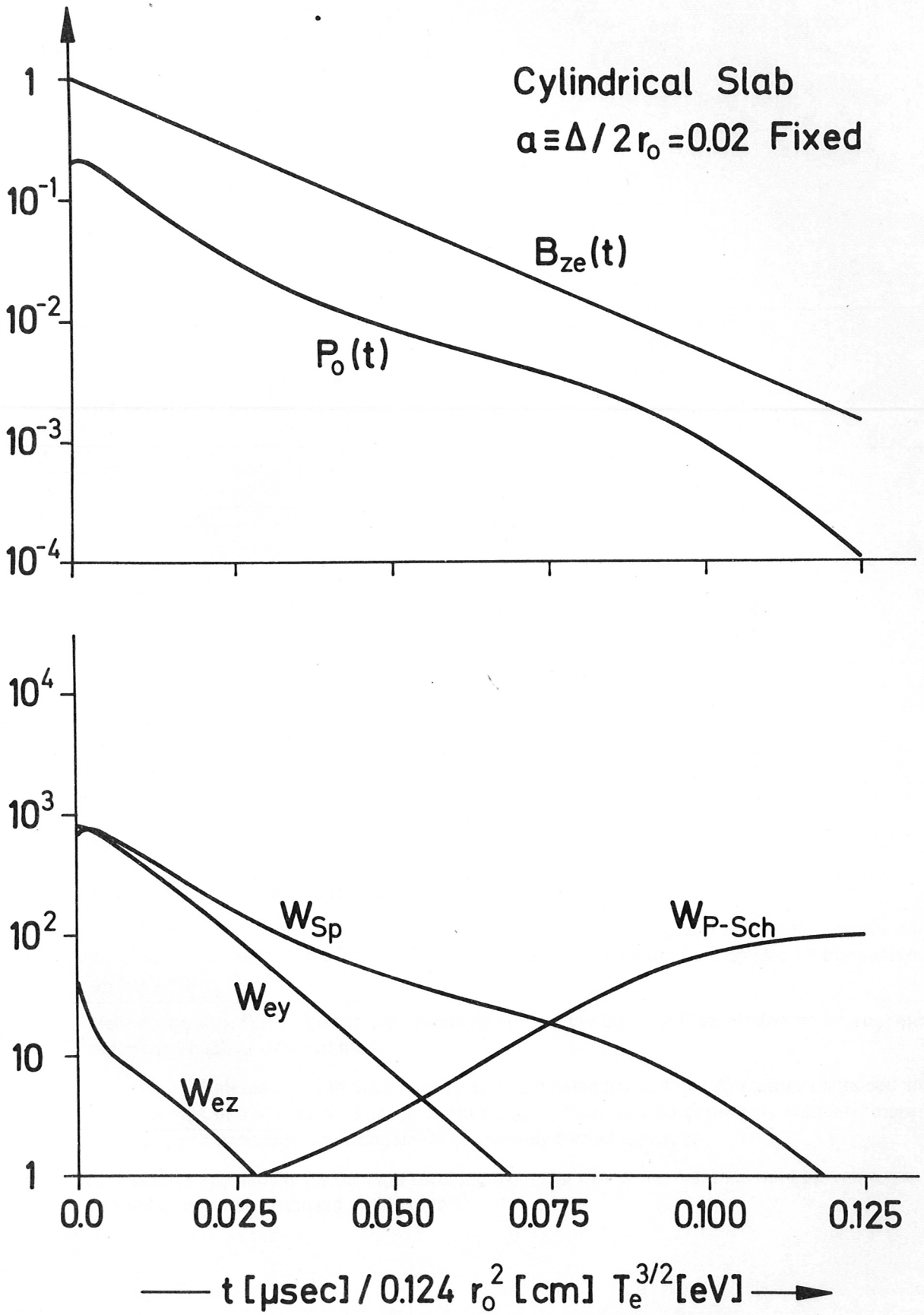
Cylindrical Slab
$a \equiv \Delta / 2 r_o = 0.02$ Fixed
$B_{ze}(t)$
$P_o(t)$
1
10^{-1}
10^{-2}
10^{-3}
10^{-4}
10^4
10^3
10^2
10
1
W_{Sp}
$W_{P\text{-}Sch}$
W_{ey}
W_{ez}
0.0
0.025
0.050
0.075
0.100
0.125
$t\,[\mu sec] / 0.124\, r_o^2\,[cm]\, T_e^{3/2}[eV]$

Fig. 9